Effect of the Indo-Pacific Warm Pool on Lower-Stratospheric Water Vapor and Comparison with the Effect of ENSO

FEI XIE,[a] XIN ZHOU,[b,c] JIANPING LI,[a,d] QUANLIANG CHEN,[b] JIANKAI ZHANG,[e] YANG LI,[b] RUIQIANG DING,[b,c] JIAQING XUE,[c] AND XUAN MA[a]

[a] *College of Global Change and Earth System Science, Beijing Normal University, Beijing, China*
[b] *Plateau Atmosphere and Environment Key Laboratory of Sichuan Province, College of Atmospheric Sciences, Chengdu University of Information Technology, Chengdu, China*
[c] *State Key Laboratory of Numerical Modeling for Atmospheric Sciences and Geophysical Fluid Dynamics (LASG), Institute of Atmospheric Physics, Chinese Academy of Sciences, Beijing, China*
[d] *Laboratory for Regional Oceanography and Numerical Modeling, Qingdao National Laboratory for Marine Science and Technology, Qingdao, China*
[e] *Key Laboratory for Semi-Arid Climate Change of the Ministry of Education, College of Atmospheric Sciences, Lanzhou University, Lanzhou, China*

(Manuscript received 25 August 2017, in final form 7 September 2017)

ABSTRACT

Time-slice experiments with the Whole Atmosphere Community Climate Model, version 4 (WACCM4), and composite analysis with satellite observations are used to demonstrate that the Indo-Pacific warm pool (IPWP) can significantly affect lower-stratospheric water vapor. It is found that a warmer IPWP significantly dries the stratospheric water vapor by causing a broad cooling of the tropopause, and vice versa for a colder IPWP. Such imprints in tropopause temperature are driven by a combination of variations in the Brewer–Dobson circulation in the stratosphere and deep convection in the troposphere. Changes in deep convection associated with El Niño–Southern Oscillation (ENSO) reportedly have a small zonal mean effect on lower-stratospheric water vapor for strong zonally asymmetric effects on tropopause temperature. In contrast, IPWP events have zonally uniform imprints on tropopause temperature. This is because equatorial planetary waves forced by latent heat release from deep convection project strongly onto ENSO but weakly onto IPWP events.

1. Introduction

Stratospheric processes can influence tropospheric weather and the climate system through both dynamical processes and the radiative effects of greenhouse gases in the stratosphere (e.g., Baldwin and Dunkerton 2001; Son et al. 2008, 2010; Xie et al. 2016; Zhang et al. 2016). Stratospheric water vapor (SWV), an important greenhouse gas, contributes significantly to global climate change by altering Earth's radiation budget (Forster and Shine 1999; Solomon et al. 2010; Dessler et al. 2013; Hegglin et al. 2014). It also influences stratospheric chemical processes, such as ozone depletion (Evans et al. 1998; Shindell 2001; Stenke and Grewe 2005; Tian et al. 2010; Anderson et al. 2012). There has been considerable interest in understanding the observed SWV variations and determining the factors that control them (Holton and Gettelman 2001; Rosenlof et al. 2001; Fueglistaler et al. 2005; Randel et al. 2006; Dhomse et al. 2008; Tian et al. 2009; Wang et al. 2014; T. Wang et al. 2015). Although the changes in SWV levels have been widely studied (Sherwood and Dessler 2000; Rosenlof 2003; Scaife et al. 2003; Fueglistaler and Haynes 2005; Jiang et al. 2007, 2015; Fu 2013; Hegglin et al. 2014), the characteristics of the SWV variations and their controlling factors remain subjects of debate.

Most of the SWV comes from tropospheric air entering the stratosphere through the tropical tropopause layer (TTL), where cold temperatures provide the primary control of its humidity (Brewer 1949; Fueglistaler et al. 2009; Randel and Jensen 2013). Variations in the SWV can be traced to variations in the tropical tropopause temperature. Within the TTL, temperatures reflect the combined influences of stratospheric (top

Corresponding author: Xin Zhou, zhouxin13@mails.ucas.ac.cn

DOI: 10.1175/JCLI-D-17-0575.1

down) and tropospheric (bottom up) processes (Highwood and Hoskins 1998; Gettelman and Forster 2002; Fueglistaler et al. 2009; Grise and Thompson 2013). It is well established that a strengthening (weakening) of the Brewer–Dobson circulation in the stratosphere (e.g., Birner and Bönisch 2011) driven by extratropical stratospheric waves should cool (warm) the tropopause (e.g., Holton et al. 1995; Fu et al. 2010). Thermally driven deep convection in the troposphere that excites equatorial planetary waves can contribute significantly to an increase in tropopause height and thereby a cooling of the TTL (e.g., Highwood and Hoskins 1998). In contrast to the extratropical stratospheric waves, the equatorial planetary waves are associated with zonal asymmetries in the TTL temperature field (Grise and Thompson 2012, 2013). Closely linked to both tropospheric convection and stratospheric circulation, variations in tropical SST play an important role in determining the TTL temperature and thus in modulating the SWV (e.g., Rosenlof and Reid 2008; Garfinkel et al. 2013a).

On interannual time scales, apart from the quasi-biennial oscillation (QBO; Dunkerton 1978; O'Sullivan and Dunkerton 1997; Randel et al. 1998; Fueglistaler and Haynes 2005; Chiou et al. 2006; Wang et al. 2013; Kawatani et al. 2014; W. K. Wang et al. 2015), the impact of variability in tropical SST associated with ENSO on the SWV has been widely discussed (Kirk-Davidoff et al. 1999; Scaife et al. 2003; Fernández et al. 2004; García et al. 2007; Xie et al. 2011, 2012; Schieferdecker et al. 2015; Hu et al. 2014, 2016; Wang et al. 2016). Anomalous tropical convection associated with El Niño excites equatorial planetary waves, including both tropical Rossby and Kelvin waves (Highwood and Hoskins 1998; Dima and Wallace 2007; Virts and Wallace 2010), which are responsible for the anomalous warm temperatures over the western Pacific and the anomalous cold temperatures over the eastern Pacific. The horseshoe pattern of the tropopause temperature patterns over the tropical western Pacific, with two almost meridionally symmetric anticyclones [Gill–Matsuno solution; see Gill (1980) and Matsuno (1966)], is a well-known feature that indicates strong equatorial planetary wave activity during ENSO events (Dima and Wallace 2007; Grise and Thompson 2012; Konopka et al. 2016). Trajectory-based studies driven by meteorological reanalysis data have shown that strong El Niño situations (e.g., 1997/98 and 2015/16) have a moistening impact in spring (Fueglistaler and Haynes 2005; Konopka et al. 2016; Avery et al. 2017), and cold ENSO events (La Niña) have a smaller drying impact (Bonazzola and Haynes 2004; Fueglistaler and Haynes 2005; Konopka et al. 2016). However, except for very strong ENSO events, the net zonal effect of ENSO on the SWV is often not clearly discernible (Fueglistaler and Haynes 2005) because of the zonally asymmetric patterns of tropopause temperature anomalies. Different flavors of El Niño, such as the eastern Pacific (EP) El Niño and central Pacific (CP) El Niño (Yu and Kao 2007; Kao and Yu 2009), lead to different tropopause temperature patterns owing to their different warm SST centers (Xie et al. 2012; Garfinkel et al. 2013c). However, in spite of the dissimilarity in the warm and cold center locations, the zonal asymmetry is quite similar in the two flavors of El Niño.

Compared to the extensively discussed SST in the eastern Pacific (e.g., Scaife et al. 2003) and the central Pacific (Ding et al. 2011; Xie et al. 2012; Garfinkel et al. 2013c; Ding and Fu 2017), the Indo-Pacific warm pool has not received adequate attention regarding its impacts on the SWV. The Indo-Pacific warm pool encompasses by far the largest expanse of warm water, with average annual temperatures exceeding 28°C (Yan et al. 1992). Vigorous atmospheric convection and "super greenhouse effect" (e.g., Raval and Ramanathan 1989; Su et al. 2006) occur over the Indo-Pacific warm pool (IPWP) for its very high background (Tompkins 2001). In addition, as one of the main contributors to the tropospheric Hadley and Walker circulations, SST variations in the IPWP not only directly affect convection in the troposphere, but they also influence circulation in the stratosphere via the modulation of extratropical planetary Rossby waves (Fletcher and Kushner 2011, 2013; Zhou et al. 2017). Therefore, a connection between the IPWP and the SWV would not be surprising. If it does exist, it is not clear whether the zonal mean effect of the IPWP would be as insignificant as its ENSO counterpart because of the zonally asymmetric response.

In this paper, we provide evidence for robust links between the alternating warming and cooling episodes of the IPWP and the SWV. In particular, our study constitutes the first attempt to investigate what distinguishes the IPWP from ENSO in its effects on the SWV. To represent the warm and cold phases of IPWP SST anomalies, we use the definitions of IPWP Niño and IPWP Niña events from Zhou et al. (2017). They have introduced an SST index called $TI_{(IPWP)}$, which is the standardized integral of the SST anomalies in the IPWP area (15°S–15°N, 90°E–180°). An IPWP Niño event is identified when a period during which the 5-month running mean of monthly $TI_{(IPWP)}$ exceeds the threshold of 0.5. The same applies for the identification of an IPWP Niña event, but using the threshold of −0.5. Zhou et al. (2017) provide a listing of IPWP Niño and Niña events from 1980 to 2015, which is also presented here in

TABLE 1. List of the IPWP Niño and IPWP Niña events from 1980 to 2015 analyzed in this paper. Numbers in parentheses are the duration of the event in months, followed by the number of months that the IPWP Niño or Niña event coincides with an ENSO event.

IPWP Niño	IPWP Niña
Nov 1982–May 1983 (7, 7)	Jun 1981–Jan 1982 (8, 0)
Nov 1986–May 1988 (19, 16)	Feb 1984–Mar 1986 (26, 9)
Oct 1990–Sep 1991 (12, 4)	Oct 1988–Apr 1993 (55, 8)
Jan 1995–Feb 1996 (14, 3)	Feb 1999–Mar 2001 (26, 25)
May 1997–Jul 1998 (15, 13)	Nov 2005–Apr 2006 (6, 0)
Dec 2001–Apr 2004 (29, 9)	Sep 2007–Nov 2008 (15, 10)
Oct 2004–Mar 2005 (6, 6)	Jul 2010–Aug 2012 (26, 17)
Jun 2009–May 2010 (12, 10)	
Jul 2014–Oct 2015 (16, 12)	

Table 1. The remainder of this paper includes both model simulations and observations and is organized as follows. The model, basic datasets, and analysis tools are described in section 2. Section 3 documents the characteristics of the SWV variations associated with IPWP Niño and Niña events and presents the potential mechanisms, including the combined effects of the top-down and bottom-up processes. In section 4, the role of the equatorial planetary waves in distinguishing the IPWP Niño and Niña events from ENSO is discussed. Finally, our conclusions are presented in section 5.

2. Simulations, data, and methods

a. Simulations

Simulations were performed with the Whole Atmosphere Community Climate Model, version 4 (WACCM4) (Marsh et al. 2013), which is a part of the Community Earth System Model (CESM) framework developed by the National Center for Atmospheric Research (Hurrell et al. 2013). WACCM4 uses a coupled system including atmosphere, ocean (Danabasoglu et al. 2012), land, and sea ice (Holland et al. 2012) components. The standard version has 66 vertical levels extending from the ground to 4.5×10^{-6} hPa (approximately 160-km geometric altitude), with a vertical resolution of 1.1–1.4 km in the tropical tropopause layer and the lower stratosphere (<30 km). All simulations use a horizontal resolution of 1.9° × 2.5° (latitude × longitude) and do not include interactive chemistry (García et al. 2007). Fixed greenhouse gas (GHG) values used in the model radiation scheme are based on emissions scenario A2 of the Intergovernmental Panel on Climate Change (IPCC) (WMO 2003) over the period 1980–2015. And the prescribed ozone forcing, with a 12-month seasonal cycle averaged over the period 1980–2015 from the CMIP5 ensemble mean ozone output, is used in our simulations. The (QBO forcing time series is determined using a 28-month fixed cycle.

A group of model integrations is used to isolate the impact of IPWP Niño and IPWP Niña on the SWV (refer to Table 2 for description of experiments). Briefly, we examined three 30-yr time-slice simulations forced by repeating annual cycles of SSTs that represent IPWP Niño and IPWP Niña. Composite SST anomalies for IPWP Niño and IPWP Niña (see Figs. 1c,d in Zhou et al. 2017) are used to force the simulations. The key point is that these model integrations provide many samples of the atmospheric response to identical SST anomalies and are long enough to achieve statistical robustness (Garfinkel et al. 2013b).

Figure 1 shows the climatological distributions of water vapor from WACCM4 simulations and Stratospheric

TABLE 2. Description of experiments R1–R9.

Experiment	Description
R1	Control run using CESM case F_2000_WACCM_SC. Prescribed SST forcing using monthly mean climatology from 1980 to 2015.
R2	As in R1, but with slightly different initial conditions. To produce different initial conditions,
R3	the CESM model parameter "pertlim" is used to produce an initial temperature perturbation, which has a magnitude on the order of 10^{-14}.
R4	As in R1, but with IPWP Niño composite anomalies (Fig. 1c in Zhou et al. 2017) added in the region 15°S–15°N, 90°E–180°, with spatial smoothing applied around the region. To prevent discontinuities in SST forcing at the IPWP boundary, SST anomalies at the boundary are added to the three grid points closest to the boundary with weights of 0.75, 0.50, and 0.25, respectively, moving away from the boundary.
R5	As in R4, but with slightly
R6	different initial conditions.
R7	As in R4, but with IPWP Niña composite anomalies (Fig. 1d in Zhou et al. 2017).
R8	As in R7, but with slightly different initial conditions.
R9	

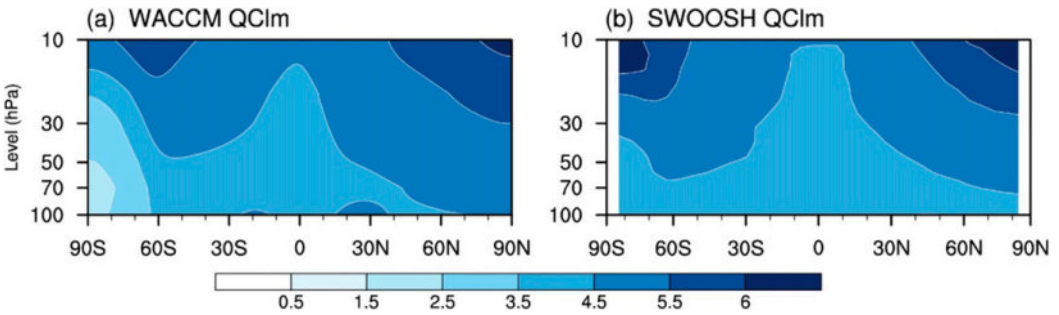

FIG. 1. Climatological water vapor (ppmv) for 1980–2015 from (a) WACCM4 simulations and (b) the SWOOSH observational dataset.

Water and Ozone Satellite Homogenized (SWOOSH) observations. The simulated zonal mean climatological SWV distribution is in good agreement with the observations. Note that the climatological WACCM4 SWV above 30 hPa is a little lower than that in SWOOSH resulting from the neglect of methane oxidation in the stratosphere in WACCM4. However, all model results in this study are obtained as the difference between two model climatologies, so the net effect of any such biases on the results of this paper should be very small.

b. Data

SST data from the Hadley Centre Sea Ice and Sea Surface Temperature dataset (HadISST), with a horizontal resolution of 1° × 1°, were used. The outgoing longwave radiation (OLR) data from 1979 to 2010 were obtained from http://www.cdc.noaa.gov/. Monthly mean wind, temperature, and geopotential height data for the period 1980–2015 from the National Centers for Environmental Prediction (NCEP)–U.S. Department of Energy (DOE) AMIP-II reanalysis and the European Centre for Medium-Range Weather Forecasts (ECMWF) interim reanalysis (ERA-Interim) were used. NCEP–DOE reanalysis data were on 17 pressure levels from 1000 to 10 hPa on a 2.5° × 2.5° horizontal grid, and ERA-Interim data were obtained as monthly mean fields from 37 discrete pressure levels on a 1.5° × 1.5° horizontal mesh (Simmons et al. 2007a,b; Uppala et al. 2008). We confirmed that the corresponding results from the two datasets are generally consistent and will only report here the results obtained from the ERA-Interim dataset. QBO and ENSO signals are removed by regressing atmospheric variables onto the QBO index and Niño index. For the QBO index, we take the standardized anomaly of equatorial 50-hPa zonal winds (anomalies in this paper are calculated by subtracting the mean seasonal cycle). Niño-3.4 and Niño-4 indices are from NCEP/CPC (http://www.cpc.ncep.noaa/gov/data/indices/ersst3b.nino.mth.ascii).

Because substantial differences are known to exist between NCEP–DOE and ECMWF reanalysis water vapor data and observations (Hamilton 1993; Gettelman et al. 2010; Jiang et al. 2015), we used observations from the SWOOSH dataset (e.g., Davis et al. 2016). The SWOOSH dataset is a merged record of SWV measurements taken by a number of limb sounding and solar occultation satellites over the past 30 years. The primary SWOOSH product is a monthly mean zonal mean gridded dataset containing ozone and water vapor data from the SAGE II/III, *Upper Atmosphere Research Satellite* (*UARS*) Halogen Occultation Experiment (HALOE), *UARS* MLS, and *Aura* MLS satellite instruments, covering the period from 1984 to the present.

c. Analysis methods

An expression for the vertical component of the Brewer–Dobson (BD) circulation in a pressure coordinate system was given by Edmon et al. (1980) as

$$\overline{\omega}^* = \overline{\omega} + (a\cos\varphi)^{-1}\{\cos\varphi[\overline{(v'\theta')}/\overline{\theta}_p]\}_\varphi,$$

where α is the radius of the earth, v is the meridional wind component, θ is the potential temperature, $\overline{\omega}$ is the zonal-mean vertical velocity in pressure coordinates, and subscripts p and φ denote derivatives with respect to pressure and latitude, respectively. The overbar denotes the zonal mean, and the prime denotes departures from the zonal mean.

The equatorial planetary wave index (EPWI; Grise and Thompson 2012) is used to represent variability in the amplitude of the equatorial planetary waves. The index is calculated using the projection of the anomalous 150-hPa zonal wind field u^* onto the seasonally varying climatological mean 150-hPa u^* over the 20°S–20°N domain (the asterisk indicates that the zonal mean has been removed from the zonal wind field).

The linear barotropic model in a steady state can be expressed in the form of the vorticity equation

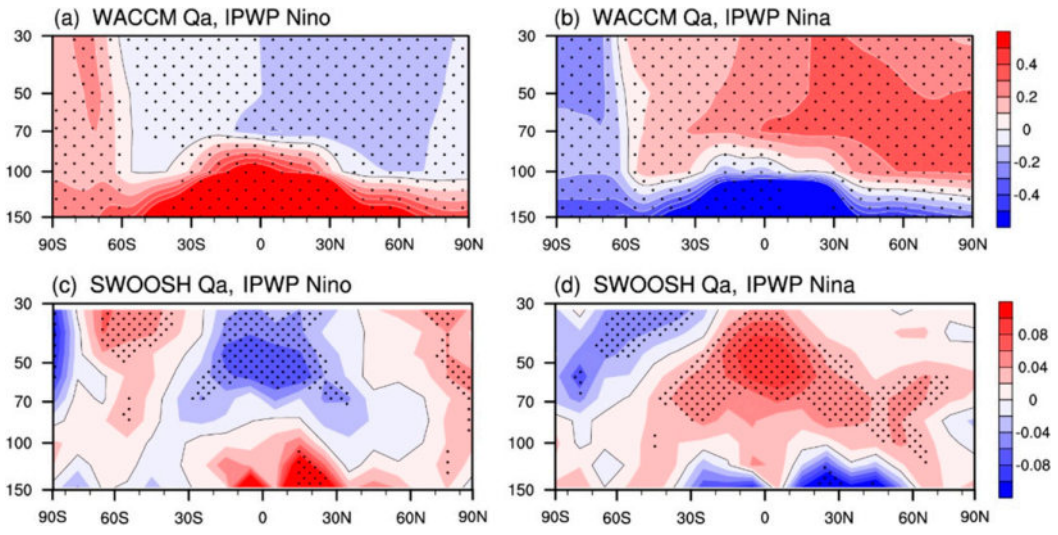

FIG. 2. Differences in zonal mean water vapor (ppmv) (a) between the ensemble mean of experiments R4–R6 and R1–R3 and (b) between the ensemble mean of experiments R7–R9 and R1–R3. Composite water vapor anomalies (ppmv) are shown for (c) IPWP Niño and (d) IPWP Niña events, based on SWOOSH data for 1980–2015. Before performing the composite analysis, ENSO and QBO signals were removed from the data. Anomalies significant at the 90% confidence level according to the Student's *t* test are stippled.

$$J(\overline{\psi}, \nabla^2\psi') + J(\psi', \nabla^2\overline{\psi} + f) + \nu\nabla^6\psi' + \alpha\nabla^2\psi' = S',$$

where J denotes a Jacobian operator, $\overline{\psi}$ and ψ' represents basic state and perturbation streamfunctions, f represents the Coriolis parameter, and S' is the anomalous vorticity forcing associated with divergent wind. The biharmonic diffusion coefficient ν is set to a damping time scale of 1 day for the smallest wave, while the Rayleigh friction coefficient α has a damping time scale of 10 days. The model is solved using a spherical harmonic expansion with T42 spectral truncation (Watanabe 2004).

The linear baroclinic model (LBM) employed in this study is constructed by linearizing the primitive equations about a 3D climatological basic state. This model has a T42 horizontal spectral resolution and 20 vertical levels on sigma coordinates with vorticity, divergence, temperature, and the logarithm of surface pressure as model variables. Details of the model formation can be found in Watanabe and Kimoto (2000). Horizontal and vertical diffusion, Newtonian damping, and Rayleigh friction are all included in the model. The biharmonic horizontal diffusion is set with a damping time scale of 1 day for the smallest wave. Weak vertical diffusion with a damping time scale of 1000 days is adopted to suppress vertical computational noise. Newtonian damping and Rayleigh friction represented as linear drag have a time scale of 0.2 days in the lower boundary layer and 30 days at midlevels. With the above dissipation setting, the model takes about 25 days to achieve a steady state. As such, the average for days 31–35 is present as the steady response.

3. Influence of IPWP variations on SWV

Figures 2a and 2b show the zonal mean anomalies of SWV forced by SST anomalies during IPWP Niño and Niña events in WACCM4 simulations. The experimental design is described in section 2. The IPWP Niño events tend to moisten the global upper troposphere (Fig. 2a) but dry the lower stratosphere, except at high latitudes in the Southern Hemisphere, and vice versa for IPWP Niña (Fig. 2b). The composite zonal mean anomalies of SWV during IPWP Niño and Niña events from SWOOSH data are shown in Figs. 2c and 2d. Note that the ENSO and QBO signals have been removed from the water vapor anomalies before the composite analysis. The results from observations support those from WACCM4 simulations, except that a positive signal of SWV is found at high latitudes in the Northern Hemisphere stratosphere. This may be because the ENSO and QBO signals in the observations cannot be removed completely using linear regression.

The zonally resolved patterns of tropical SWV anomalies are further presented in Fig. 3. The results correspond well to the zonal mean anomalies of SWV in Fig. 2, confirming that IPWP Niño (Niña) events can significantly dry (moisten) the lower stratosphere. In particular, there are maximum negative and positive water vapor anomalies located in the lower stratosphere over the IPWP region in WACCM4 for IPWP Niño and IPWP Niña events, respectively (Figs. 3a,b). These features can also be recognized in the SWOOSH data but

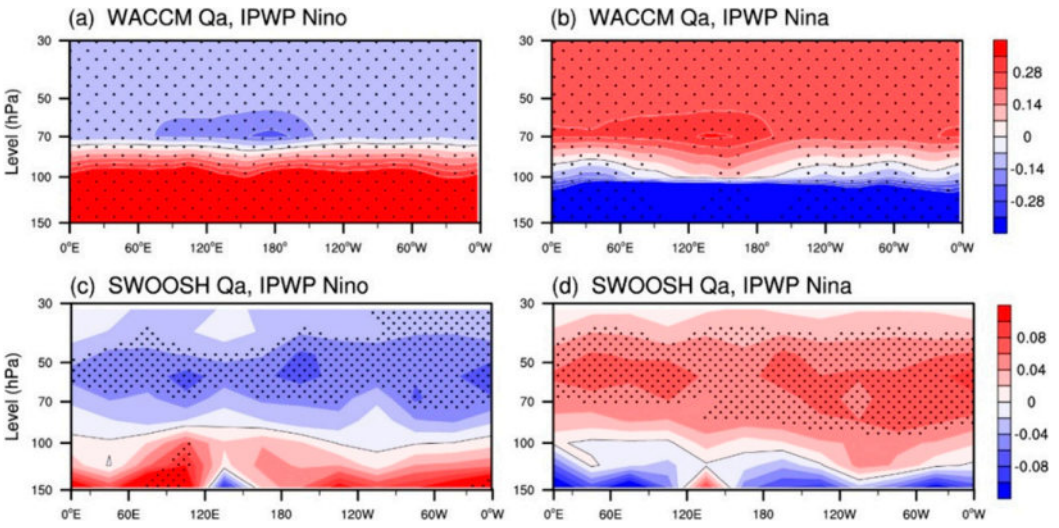

FIG. 3. As in Fig. 2, but for meridional mean water vapor (averaged over 30°S–30°N).

are not as obvious as in the WACCM4 simulations, probably due to the limited spatiotemporal resolution in the upper troposphere and lower stratosphere.

In the stratosphere, IPWP-induced fluctuations in the tropical BD circulation are strengthened during IPWP Niño events and suppressed during IPWP Niña events (Fig. 4). The calculation of the BD circulation is presented in section 2. Results from model simulations (Figs. 4a,b) and composite analysis using the ERA-Interim dataset (Figs. 4c,d) are in close agreement. This implies a strengthened (weakened) mass flux transport from the tropical troposphere to the stratosphere during IPWP Niño (Niña) events. However, why does IPWP Niño correspond to a decrease in SWV, and IPWP Niña correspond to an increase?

The variations in the SWV, as mentioned in section 1, can be traced mainly to variations in the tropical

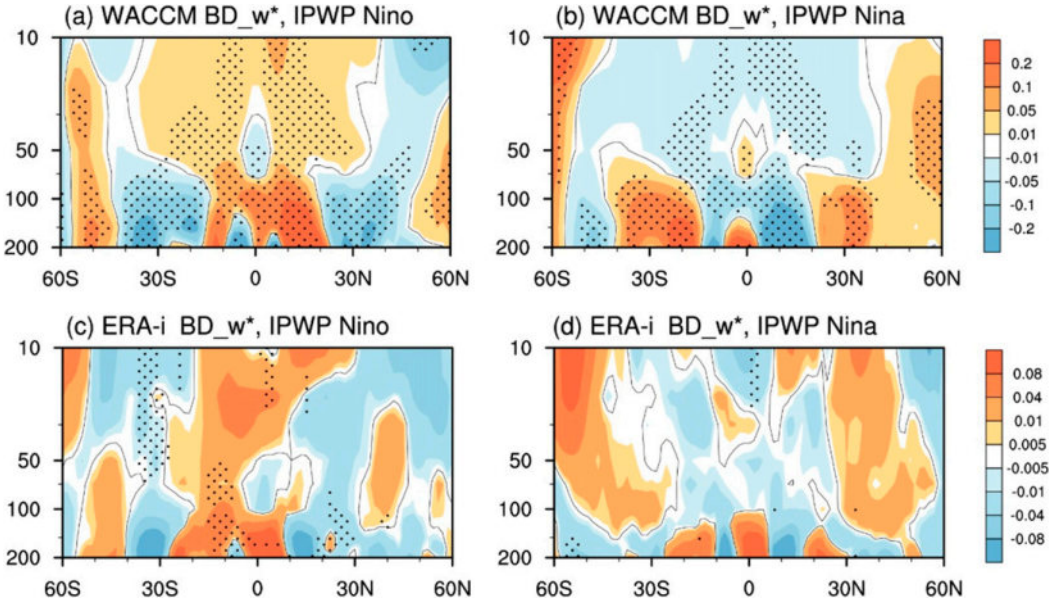

FIG. 4. Difference in vertical velocity of BD circulation (mPa s^{-1}) (a) between the ensemble mean of experiments R4–R6 and R1–R3 and (b) between the ensemble mean of experiments R7–R9 and R1–R3. Composite vertical velocity anomalies of BD circulation (mPa s^{-1}) are shown for (c) IPWP Niño and (d) IPWP Niña from ERA-Interim for 1980–2015. Before performing the composite analysis, ENSO and QBO signals were removed from the data. Anomalies significant at the 90% confidence level according to the Student's *t* test are stippled.

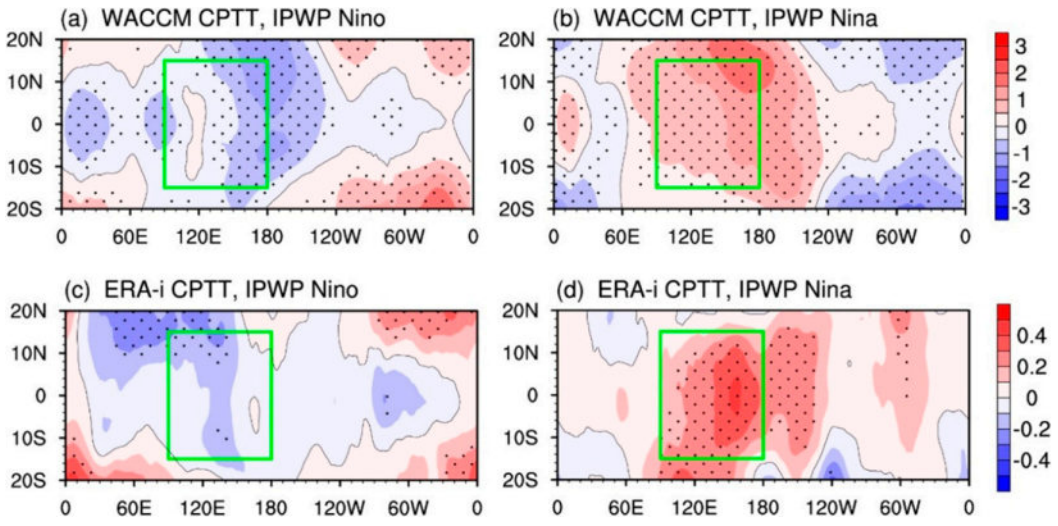

FIG. 5. Tropical CPTT (°C) differences (a) between the ensemble mean of experiments R4–R6 and R1–R3 and (b) between the ensemble mean of experiments R7–R9 and R1–R3. Composite tropical CPTT anomalies are shown for (c) IPWP Niño and (d) IPWP Niña events from ERA-Interim for 1980–2015. The tropical CPTT is calculated as the lowest air temperature between 500 and 50 hPa. The integration time step of the model simulation is 30 min, but monthly air temperature output is used to calculate CPTT. Before performing the composite analysis, ENSO and QBO signals were removed from the data. Anomalies significant at the 90% confidence level according to the Student's *t* test, are stippled. The green rectangle is the IPWP region.

tropopause temperature. Figure 5 shows the patterns of cold-point tropopause temperature (CPTT) anomalies associated with IPWP Niño and Niña events from WACCM4 results and the ERA-Interim dataset. The patterns highlight the nearly uniform broad cooling and warming during IPWP Niño and Niña events, respectively, with anomalous centers located over the IPWP. The significant cooling and warming effects on the CPTT during IPWP Niño and Niña events contribute to the robust drying and wetting signals in the SWV. Figure 6 presents the lower SWV anomalies during IPWP Niño and Niña events from simulations and observations. It clarifies the broad drying (moistening) effect of IPWP Niño (Niña) on the lower stratosphere with an anomalous center over the vicinity of the IPWP. The patterns of SWV anomalies resemble the patterns of the CPTT (Fig. 5). This result implies that the CPTT changes in IPWP Niño and Niña events dominate variations in SWV, contributing to the significant zonal mean anomalies of SWV in Fig. 2.

The top-down process in the tropopause layer, involving large-scale ascent of tropical air driven by a strengthened BD circulation (e.g., Highwood and Hoskins 1998; Gettelman and Forster 2002; Fueglistaler et al. 2009), leads to anomalous cooling in the tropopause during IPWP Niño. The reverse applies for IPWP Niña. In the bottom-up process in the troposphere (e.g., Fu 2013; Grise and Thompson 2013), deep convection, together with low-level (850 hPa) wind anomalies, develops in response to the warm and cold IPWP events, as seen in simulations and observations (Fig. 7). During IPWP Niño (Figs. 7a,c), easterly trade winds are enhanced as a result of the convergence of zonal winds associated with Kelvin and Rossby waves toward the heat source (Matsuno 1966; Gill 1980), and vice versa for IPWP Niña (Figs. 7b,d). This indicates a strengthened (weakened) upwelling over the IPWP region during warm (cold) events, so more (less) deep convection over this region is expected. Figure 8 presents the OLR anomalies associated with IPWP Niño and Niña from simulations and observations. Here the magnitude of OLR is used as a proxy for the intensity of convective activity. During IPWP Niño events, enhanced convection (negative OLR anomalies) occurs over the IPWP region, which is evident in both WACCM4 simulations and the NCEP–DOE reanalysis data. The enhanced upwelling in the tropical upper troposphere (bottom-up process), combined with a strengthened BD circulation in the stratosphere (top-down process), leads to a cooling around the tropopause during IPWP Niño and thereby results in the zonal mean anomalies of SWV (Fig. 2). The reverse chain holds for IPWP Niña.

The significant effects of IPWP Niño and Niña on zonal mean SWV (Fig. 2) differ from the small zonal mean effects of ENSO (Scaife et al. 2003; Bonazzola and Haynes 2004; Fueglistaler and Haynes 2005). In brief, the fairly uniform, out-of-phase patterns of CPTT during IPWP Niño and Niña are different from the zonal

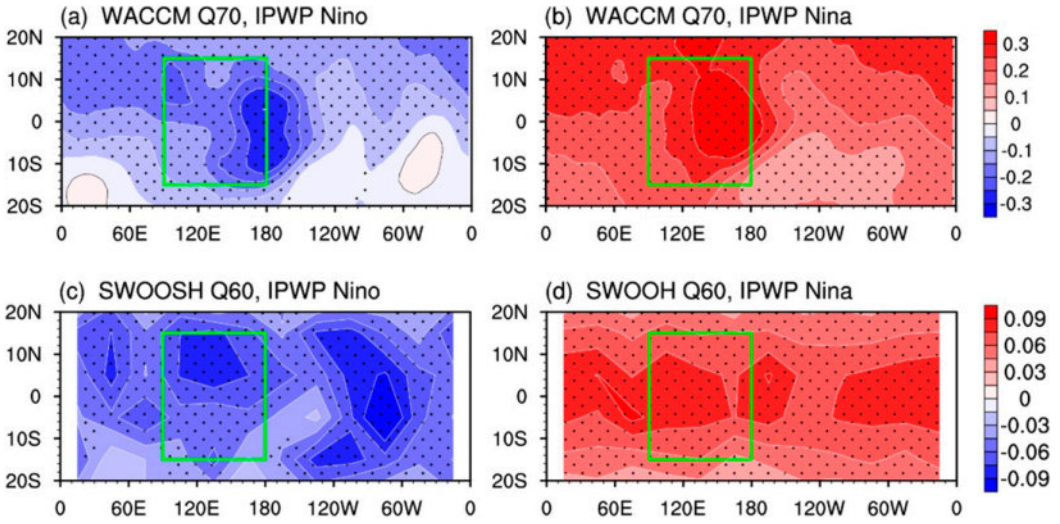

FIG. 6. Tropical 70-hPa water vapor (ppmv) differences (a) between the ensemble mean of experiments R4–R6 and R1–R3 and (b) between the ensemble mean of experiments R7–R9 and R1–R3. Composite 60-hPa water vapor (ppmv) anomalies are shown for (c) IPWP Niño and (d) IPWP Niña events from SWOOSH data for 1980–2015. Before performing the composite analysis, ENSO and QBO signals were removed from the data. Anomalies significant at the 90% confidence level according to the Student's t test are stippled. The green rectangle is the IPWP region.

dipole patterns associated with ENSO, leading to the distinctly different signatures in the SWV of IPWP Niño/Niña and ENSO.

According to the analysis above, IPWP-related anomalies of the BD circulation and deep convection (top-down and bottom-up processes) are responsible for the zonal mean patterns of tropopause temperature during IPWP warm and cold events. However, the mechanisms for the zonal asymmetries of CPTT anomalies, with small amplitude in IPWP events but large

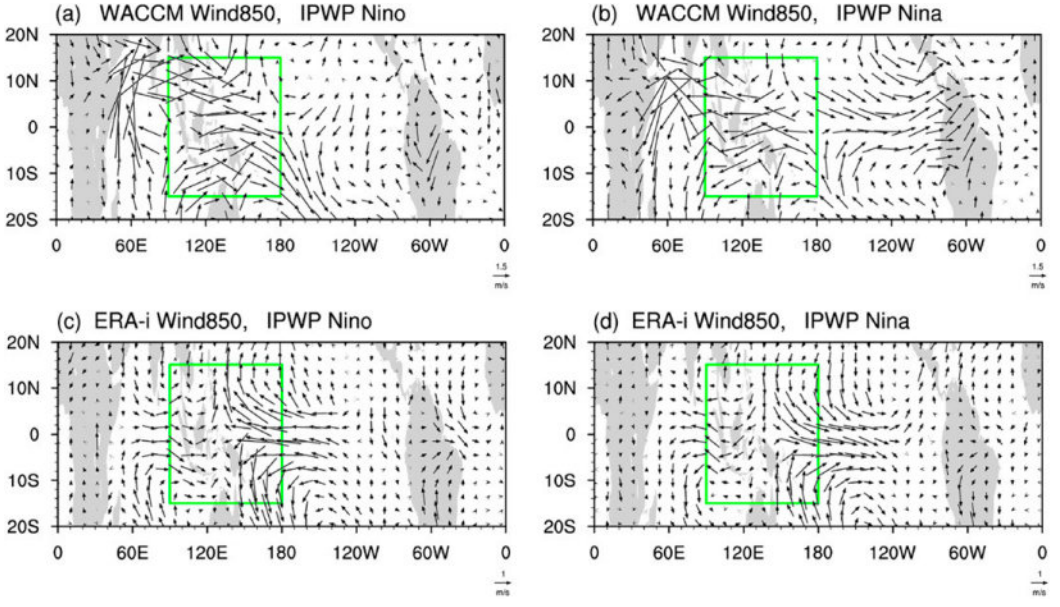

FIG. 7. Tropical low-level (850 hPa) wind (vectors; m s^{-1}) differences (a) between the ensemble mean of experiments R4–R6 and R1–R3 and (b) between the ensemble mean of experiments R7–R9 and R1–R3. Composite low-level (850 hPa) wind (vectors; m s^{-1}) anomalies are shown for (c) IPWP Niño and (d) IPWP Niña events from ERA-Interim for 1980–2015. The green rectangle is the IPWP region.

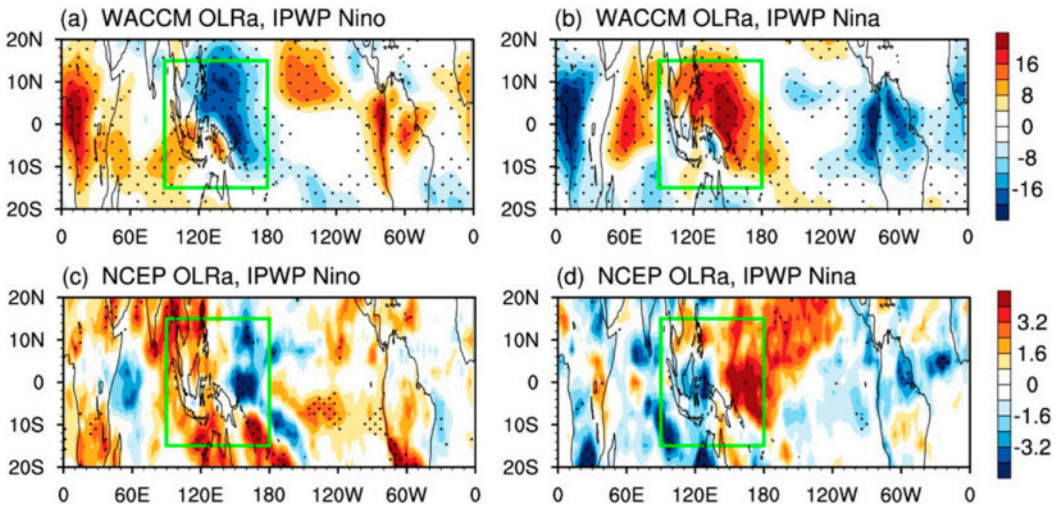

FIG. 8. Tropical OLR (W m^{-2}) differences (a) between the ensemble mean of experiments R4–R6 and R1–R3 and (b) between the ensemble mean of experiments R7–R9 and R1–R3. Composite OLR (W m^{-2}) anomalies are shown for (c) IPWP Niño and (d) IPWP Niña events from NCEP–DOE reanalysis for 1979–2012. Before performing the composite analysis, ENSO and QBO signals were removed from the data. Anomalies significant at the 90% confidence level according to the Student's *t* test are stippled. The green rectangle is the IPWP region.

amplitude in ENSO, have yet to be identified, as the IPWP and ENSO events show some similarities in the two processes; that is, the warm (cold) ENSO phase also induces a strengthened (weakened) BD circulation and increased (decreased) deep convection (e.g., Hoerling et al. 1997; Scaife et al. 2003; García-Herrera et al. 2006; Camp and Tung 2007; Marsh and García 2007; Cagnazzo et al. 2009; Ineson and Scaife 2009; Randel et al. 2009; Calvo et al. 2010; Xie et al. 2011; Ren et al. 2012, 2017; Butler et al. 2014). Why are the effects of IPWP events different from those of ENSO on zonal asymmetries of CPTT response? In the rest of this paper, we will investigate the causes of the zonal asymmetries associated with IPWP and ENSO events.

4. Possible mechanism for small zonal asymmetries of IPWP imprints on lower SWV

Tropical deep convection causes divergence of latent heat in the upper troposphere and subsequently excites equatorial planetary waves in the form of Kelvin and equatorial Rossby wave responses (Dima et al. 2005; Dima and Wallace 2007). According to Grise and Thompson (2013), the equatorial planetary waves dominate the zonally asymmetric component of the TTL temperature field. A possible reason for IPWP and ENSO imprints on CPTT having different zonal structures is that the intensity of the equatorial planetary wave activity during IPWP events differs from that during ENSO events. If the intensity during IPWP events is much weaker than during ENSO events, CPTT patterns during IPWP events should have less zonal asymmetry than during ENSO events.

To quantify the amplitude of equatorial planetary waves during IPWP and ENSO events, the EPWI (refer to section 2 for its definition) is used (Grise and Thompson 2012). The signatures of equatorial planetary waves in tropospheric circulation and temperature are obtained by regressing these variables onto the EPWI time series. Figure 9 shows the regressions of 100-hPa geopotential height, wind, and temperature onto the EPWI time series calculated from the ensemble experiments R4–R6 and R7–R9. It is found that relatively weak responses of equatorial Rossby waves and Kelvin waves to IPWP Niño and Niña are evident in the geopotential height and wind fields (Figs. 9a,c). In particular, the signature of equatorial planetary waves in tropopause temperature (Figs. 9b,d) exhibits very weak zonal asymmetries. In contrast, previous studies provide irrefutable evidence for pronounced zonally asymmetric features in the tropospheric circulation and temperature caused by equatorial planetary waves during ENSO events (Dima and Wallace 2007; Grise and Thompson 2012; Konopka et al. 2016). Thus, the differences between the imprints in the TTL during IPWP Niño/Niña and ENSO events may largely be attributed to the equatorial planetary waves.

The signatures of the equatorial planetary waves in the TTL, weak during IPWP Niño and Niña events but strong during ENSO events, are further verified in observations (Fig. 10). Here, we apply a decomposition method to calculate the contribution of the equatorial

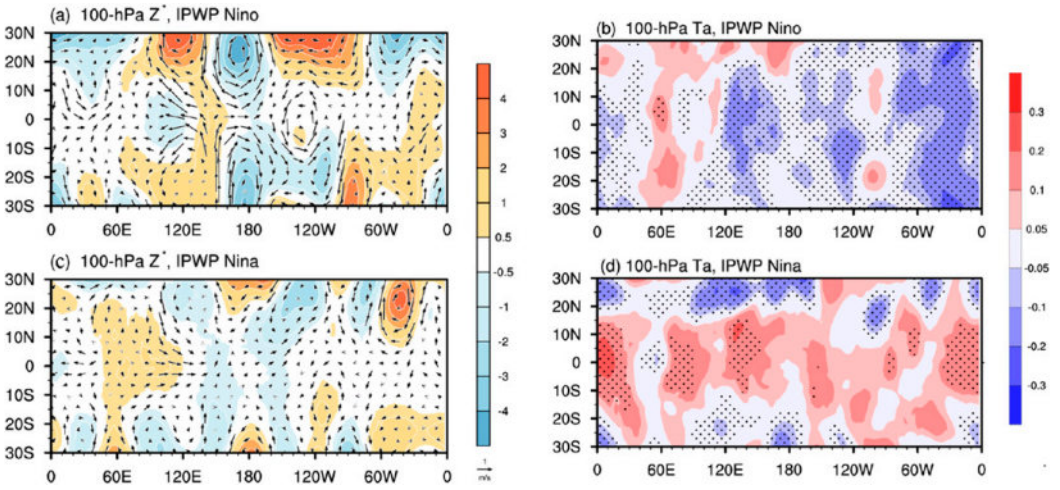

FIG. 9. (a),(c) Regression of 100-hPa geopotential height (color shading; gpm) and 100-hPa wind (vectors; m s^{-1}) onto the EPWI time series derived from (a) the ensemble mean of experiments R4–R6 (IPWP Niño case) and (c) the ensemble mean of experiments R7–R9 (IPWP Niña case). (b),(d) As in (a),(c), but for 100-hPa temperature anomalies (°C). In (b),(d), anomalies significant at the 90% confidence level according to the Student's *t* test are stippled.

planetary waves to the imprints of IPWP Niño/Niña and ENSO in the TTL. The decomposed part is derived as follows: 1) 100-hPa geopotential height and wind are regressed onto the standardized $TI_{(IPWP)}$ and Niño-3.4 indices to yield time series of geopotential height and wind anomalies that are congruent with IPWP Niño/Niña and ENSO events [$TI_{(IPWP)}$ is defined in section 1.]; and 2) the time series are regressed onto the EPWI time series to obtain regressions congruent with EPWI. Consistent with the above analysis, the signal of equatorial planetary waves is rather weak in IPWP Niño and Niña cases (Fig. 10a), revealing the weak contribution of equatorial planetary waves to imprints in the TTL. However, in the ENSO case, the horseshoe pattern associated with Kelvin waves—and to its west, the equatorial Rossby wave pattern—all reflect a strong projection of the amplitude of the equatorial planetary waves onto imprints of ENSO, in good agreement with previous research (Dima and Wallace 2007; Grise and Thompson 2012; Konopka et al. 2016).

Recently, Goss and Feldstein (2017) found that the response of extratropical planetary waves to similar spatial patterns of tropical convective anomalies varies considerably for different locations of the primary heating source. The IPWP Niño and Niña events and ENSO events affect the atmosphere differently because they drive anomalous deep convection in the troposphere at different locations. IPWP Niño excites deep convection over the IPWP region, but El Niño favors convection over the equatorial central Pacific. This difference is likely to correspond to different responses of the equatorial planetary waves.

To elucidate the responses of the equatorial planetary waves to anomalous deep convection during IPWP and ENSO events, an intermediate complexity LBM is employed (see section 2). The model is linearized about

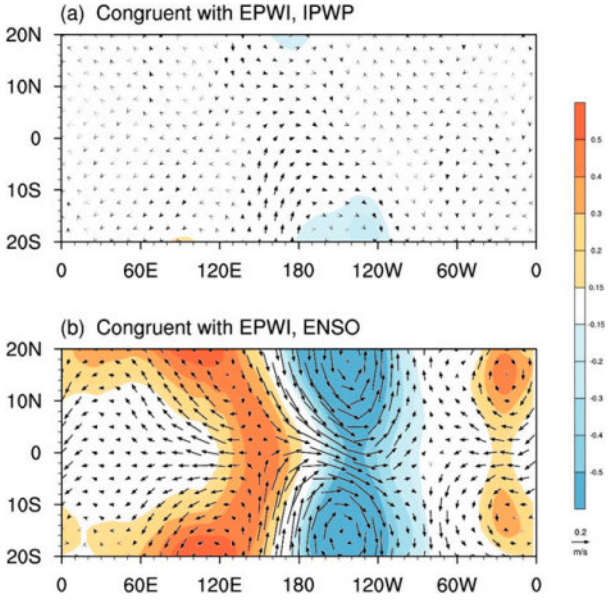

FIG. 10. Component of the regression on (a) $TI_{(IPWP)}$ and (b) Niño-3.4 that is linearly congruent with the EPWI time series. The color shading represents 100-hPa eddy geopotential height anomalies (gpm). The vectors represent 100-hPa eddy wind anomalies (m s^{-1}). The EPWI time series are derived from the monthly mean 150-hPa anomalies from ERA-Interim for 1980–2015. The $TI_{(IPWP)}$ and Niño 3.4 time series are standardized before regression.

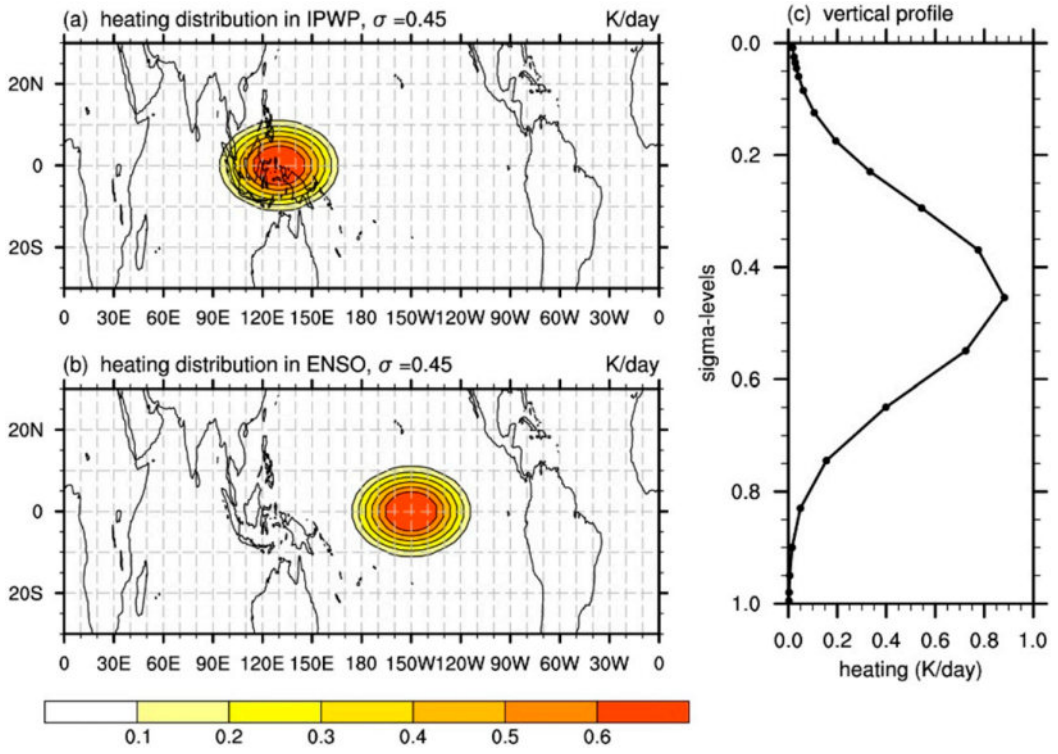

FIG. 11. Horizontal distribution of the idealized diabatic heating (K day^{-1}) at the 0.45 sigma level used in the LBM experiment for (a) IPWP Niño and (b) El Niño events. Contour/shading intervals are 0.1 K day^{-1}. (c) Vertical profile of heat source (K day^{-1}) with center point on the equator at 130°E for IPWP Niño and at 30°W for El Niño.

the 3D climatological basic state in boreal winter. An idealized diabatic heating pattern of IPWP is determined with reference to the SST and anomalous convection (Fig. 9). In the experiment for the IPWP Niño case, the heating is located in the IPWP region centered on the equator at 130°E, while in the experiment for El Niño, the idealized diabatic heating pattern has its center on the equator at 30°W, as in the classic El Niño experiment in Watanabe and Kimoto (2000). The heating patterns have elliptical cosine-squared horizontal distributions in latitude and longitude and a gamma profile in the vertical direction, with peak value at 400 hPa (model level $\sigma = 0.45$) (Rodwell and Hoskins 1996; Matthews et al. 2004). Figures 11a and 11b depict the horizontal distribution of heating at the 0.45 sigma level for the IPWP Niño case and El Niño case, respectively, with a maximum heating rate of approximately 0.6 K day^{-1} in both cases. The vertical profile of heating at the center point used in both the IPWP Niño and El Niño cases is presented in Fig. 11c. The tropical atmospheric response at 100 hPa to the idealized diabatic heating in the LBM is displayed as eddy geopotential height anomalies and eddy streamfunction anomalies in Fig. 12. The amplitudes of eddy geopotential height anomalies and eddy streamfunction anomalies in the El Niño case are more than twice as strong as those in the IPWP Niño case. The corresponding IPWP Niña and La Niña cases, with negative diabatic heating anomalies, show the same spatial patterns as in the IPWP Niño and El Niño cases, respectively, but with anomalies of opposite sign (not shown). The disparity clearly demonstrates that the equatorial planetary waves excited by ENSO are of larger magnitude than those excited by IPWP Niño and Niña. The experiments with diabatic heating forcing in the LBM further confirm the result; that is, the equatorial waves have a primary role in making the imprint of IPWP Niño and Niña on the TTL different from that of ENSO.

5. Summary

In this study, significant out-of-phase variations in the lower SWV associated with IPWP Niño and Niña events are revealed with WACCM4 experiments and composite analysis using satellite observations. The variations in the SWV are traced to variations in tropopause temperature, which show similar anomaly structures. IPWP Niño significantly cools the tropopause and subsequently dries the stratosphere through a combination of a stratospheric

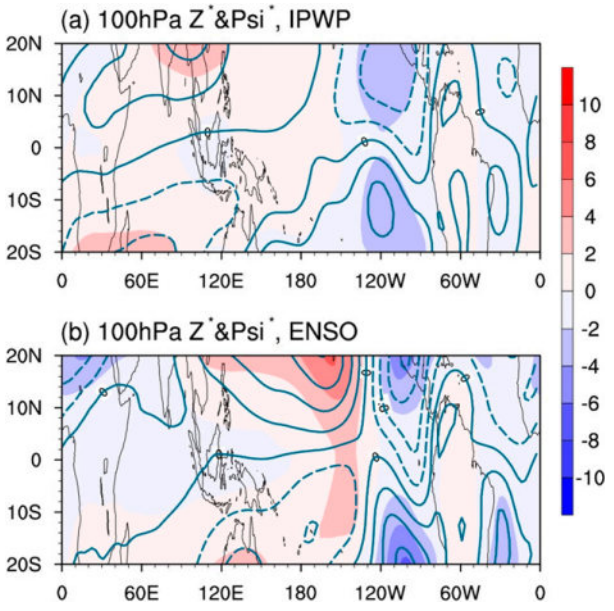

FIG. 12. Response of 100-hPa eddy geopotential height (color shading; gpm) and streamfunction (blue contours; $10^{-6}\,m^2\,s^{-1}$, contour interval of $0.4 \times 10^{-6}\,m^2\,s^{-1}$) to the specified diabatic heating forcing for (a) IPWP Niño and (b) El Niño in the LBM.

process in the form of a strengthened BD circulation and a tropospheric process via intense deep convection. The reverse chain holds for IPWP Niña.

Remarkably, the imprints in the TTL, as well as in the SWV, of IPWP Niño and Niña exhibit fairly zonally symmetric patterns. They are distinct from the imprints of ENSO, which have large zonal asymmetries, leading to very small zonal mean effects on TTL and lower SWV. Motivated by the unique signature of IPWP Niño and Niña in the SWV and TTL, we further explore the possible driving mechanisms. Anomalous tropical deep convection excites equatorial planetary waves in the form of Kelvin and equatorial Rossby wave responses, which dominate the zonally asymmetric component of the TTL temperature field (Grise and Thompson 2013). In contrast to ENSO events, the amplitude of the equatorial planetary waves projects weakly onto IPWP Niño and Niña imprints in the TTL. This weak signature of the equatorial planetary waves during IPWP Niño and Niña events is demonstrated in WACCM4 results, regression analysis using a reanalysis dataset, and experiments using an intermediate complexity LBM. Accordingly, the anomalous equatorial planetary waves are shown to be the main reason for the difference in the zonal signatures in the TTL between IPWP events and ENSO.

Acknowledgments. This work was jointly supported by the SOA International Cooperation Program on Global Change and Air–Sea Interactions (Grant GASI-IPOVAI-03) and the National Natural Science Foundation of China (Grant 41575039). Datasets were obtained from the NOAA/Climate Prediction Center, the ECMWF, SWOOSH, and the Met Office Hadley Centre. The authors thank NCAR for providing the WACCM4 model (https://www2.cesm.ucar.edu/ models/current) and appreciate the assistance provided by Prof. Masahiro Watanabe in running the linear baroclinic model.

REFERENCES

Anderson, J. G., D. M. Wilmouth, J. B. Smith, and D. S. Sayres, 2012: UV dosage levels in summer: Increased risk of ozone loss from convectively injected water vapor. *Science*, **337**, 835–839, https://doi.org/10.1126/science.1222978.

Avery, M. A., S. M. Davis, K. H. Rosenlof, H. Ye, and A. Dessler, 2017: Large anomalies in lower stratospheric water vapour and ice during the 2015–2016 El Niño. *Nat. Geosci.*, **10**, 405–409, https://doi.org/10.1038/ngeo2961.

Baldwin, M. P., and T. J. Dunkerton, 2001: Stratospheric harbingers of anomalous weather regimes. *Science*, **294**, 581–584, https://doi.org/10.1126/science.1063315.

Birner, T., and H. Bönisch, 2011: Residual circulation trajectories and transit times into the extratropical lowermost stratosphere. *Atmos. Chem. Phys.*, **11**, 817–827, https://doi.org/10.5194/acp-11-817-2011.

Bonazzola, M., and P. H. Haynes, 2004: A trajectory-based study of the tropical tropopause region. *J. Geophys. Res.*, **109**, D20112, https://doi.org/10.1029/2003JD004356.

Brewer, A. W., 1949: Evidence for a world circulation provided by the measurements of helium and water vapour distribution in the stratosphere. *Quart. J. Roy. Meteor. Soc.*, **75**, 351–363, https://doi.org/10.1002/qj.49707532603.

Butler, A. H., L. M. Polvani, and C. Deser, 2014: Separating the stratospheric and tropospheric pathways of El Niño–Southern Oscillation teleconnections. *Environ. Res. Lett.*, **9**, 024014, https://doi.org/10.1088/1748-9326/9/2/024014.

Cagnazzo, C., and Coauthors, 2009: Northern winter stratospheric temperature and ozone responses to ENSO inferred from an ensemble of Chemistry Climate Models. *Atmos. Chem. Phys.*, **9**, 8935–8948, https://doi.org/10.5194/acp-9-8935-2009.

Calvo, N., R. R. García, W. J. Randel, and D. R. Marsh, 2010: Dynamical mechanism for the increase in tropical upwelling in the lowermost tropical stratosphere during warm ENSO events. *J. Atmos. Sci.*, **67**, 2331–2340, https://doi.org/10.1175/2010JAS3433.1.

Camp, C. D., and K. K. Tung, 2007: Stratospheric polar warming by ENSO in winter: A statistical study. *Geophys. Res. Lett.*, **34**, L04809, https://doi.org/10.1029/2006GL028521.

Chiou, E. W., L. W. Thomason, and W. P. Chu, 2006: Variability of stratospheric water vapor inferred from SAGE II, HALOE, and Boulder (Colorado) balloon measurements. *J. Climate*, **19**, 4121–4133, https://doi.org/10.1175/JCLI3841.1.

Danabasoglu, G., S. C. Bates, B. P. Briegleb, S. R. Jayne, M. Jochum, W. G. Large, S. Peacock, and S. G. Yeager, 2012: The CCSM4 ocean component. *J. Climate*, **25**, 1361–1389, https://doi.org/10.1175/JCLI-D-11-00091.1.

Davis, S. M., and Coauthors, 2016: The Stratospheric Water and Ozone Satellite Homogenized (SWOOSH) database: A long-term database for climate studies. *Earth Syst. Sci. Data*, **8**, 461–490, https://doi.org/10.5194/essd-8-461-2016.

Dessler, A. E., M. R. Schoeberl, T. Wang, S. M. Davis, and K. H. Rosenlof, 2013: Stratospheric water vapor feedback. *Proc. Natl. Acad. Sci. USA*, **110**, 18 087–18 091, https://doi.org/10.1073/pnas.1310344110.

Dhomse, S., M. Weber, and J. Burrows, 2008: The relationship between tropospheric wave forcing and tropical lower stratospheric water vapor. *Atmos. Chem. Phys.*, **8**, 471–480, https://doi.org/10.5194/acp-8-471-2008.

Dima, I. M., and J. M. Wallace, 2007: Structure of the annual-mean equatorial planetary waves in the ERA-40 reanalyses. *J. Atmos. Sci.*, **64**, 2862–2880, https://doi.org/10.1175/JAS3985.1.

——, ——, and I. Kraucunas, 2005: Tropical zonal momentum balance in the NCEP reanalyses. *J. Atmos. Sci.*, **62**, 2499–2513, https://doi.org/10.1175/JAS3486.1.

Ding, Q. H., and Q. Fu, 2017: A warming tropical central Pacific dries the lower stratosphere. *Climate Dyn.*, https://doi.org/10.1007/s00382-017-3774-y, in press.

——, E. J. Steig, D. S. Battisti, and M. Küttel, 2011: Winter warming in West Antarctica caused by central tropical Pacific warming. *Nat. Geosci.*, **4**, 398–403, https://doi.org/10.1038/ngeo1129.

Dunkerton, T., 1978: On the mean meridional mass motions of the stratosphere and mesosphere. *J. Atmos. Sci.*, **35**, 2325–2333, https://doi.org/10.1175/1520-0469(1978)035<2325:OTMMMM>2.0.CO;2.

Edmon, H. J., B. J. Hoskins, and M. E. McIntyre, 1980: Eliassen-Palm cross sections for the troposphere. *J. Atmos. Sci.*, **37**, 2600–2616, https://doi.org/10.1175/1520-0469(1980)037<2600:EPCSFT>2.0.CO;2.

Evans, S. J., R. Toumi, J. E. Harries, M. P. Chipperfield, and J. M. Russell, 1998: Trends in stratospheric humidity and the sensitivity of ozone to these trends. *J. Geophys. Res.*, **103**, 8715–8725, https://doi.org/10.1029/98JD00265.

Fernández, N. C., R. R. García, R. G. Herrera, D. G. Puyol, L. G. Presa, E. H. Martín, and P. R. Rodríguez, 2004: Analysis of the ENSO signal in tropospheric and stratospheric temperatures observed by MSU, 1979–2000. *J. Climate*, **17**, 3934–3946, https://doi.org/10.1175/1520-0442(2004)017<3934:AOTESI>2.0.CO;2.

Fletcher, C. G., and P. J. Kushner, 2011: The role of linear interference in the annular mode response to tropical SST forcing. *J. Climate*, **24**, 778–794, https://doi.org/10.1175/2010JCLI3735.1.

——, and ——, 2013: Linear interference and the northern annular mode response to tropical SST forcing: Sensitivity to model configuration. *J. Geophys. Res. Atmos.*, **118**, 4267–4279, https://doi.org/10.1002/jgrd.50385.

Forster, P. M. de F., and K. P. Shine, 1999: Stratospheric water vapour changes as a possible contributor to observed stratospheric cooling. *Geophys. Res. Lett.*, **26**, 3309–3312, https://doi.org/10.1029/1999GL010487.

Fu, Q., 2013: Ocean–atmosphere interactions: Bottom up in the tropics. *Nat. Climate Change*, **3**, 957–958, https://doi.org/10.1038/nclimate2039.

——, S. Solomon, and P. Lin, 2010: On the seasonal dependence of tropical lower-stratospheric temperature trends. *Atmos. Chem. Phys.*, **10**, 2643–2653, https://doi.org/10.5194/acp-10-2643-2010.

Fueglistaler, S., and P. H. Haynes, 2005: Control of interannual and longer-term variability of stratospheric water vapor. *J. Geophys. Res.*, **110**, D24108, https://doi.org/10.1029/2005JD006019.

——, M. Bonazzola, P. H. Haynes, and T. Peter, 2005: Stratospheric water vapor predicted from the Lagrangian temperature history of air entering the stratosphere in the tropics. *J. Geophys. Res.*, **110**, D08107, https://doi.org/10.1029/2004JD005516.

——, A. Dessler, T. Dunkerton, I. Folkins, Q. Fu, and P. W. Mote, 2009: Tropical tropopause layer. *Rev. Geophys.*, **47**, RG1004, https://doi.org/10.1029/2008RG000267.

García, R. R., D. R. Marsh, D. E. Kinnison, B. A. Boville, and F. Sassi, 2007: Simulation of secular trends in the middle atmosphere, 1950–2003. *J. Geophys. Res.*, **112**, D09301, https://doi.org/10.1029/2006JD007485.

García-Herrera, R., N. Calvo, R. R. García, and M. A. Giorgetta, 2006: Propagation of ENSO temperature signals into the middle atmosphere: A comparison of two general circulation models and ERA-40 reanalysis data. *J. Geophys. Res.*, **111**, D06101, https://doi.org/10.1029/2005JD006061.

Garfinkel, C. I., D. W. Waugh, L. D. Oman, L. Wang, and M. M. Hurwitz, 2013a: Temperature trends in the tropical upper troposphere and lower stratosphere: Connections with sea surface temperatures and implications for water vapor and ozone. *J. Geophys. Res. Atmos.*, **118**, 9658–9672, https://doi.org/10.1002/jgrd.50772.

——, M. M. Hurwitz, D. W. Waugh, and A. H. Butler, 2013b: Are the teleconnections of central Pacific and eastern Pacific El Niño distinct in boreal wintertime? *Climate Dyn.*, **41**, 1835–1852, https://doi.org/10.1007/s00382-012-1570-2.

——, ——, L. D. Oman, and D. W. Waugh, 2013c: Contrasting effects of central Pacific and eastern Pacific El Niño on stratospheric water vapor. *Geophys. Res. Lett.*, **40**, 4115–4120, https://doi.org/10.1002/grl.50677.

Gettelman, A., and P. M. de F. Forster, 2002: A climatology of the tropical tropopause layer. *J. Meteor. Soc. Japan*, **80**, 911–924, https://doi.org/10.2151/jmsj.80.911.

——, and Coauthors, 2010: Multimodel assessment of the upper troposphere and lower stratosphere: Tropics and global trends. *J. Geophys. Res.*, **115**, D00M08, https://doi.org/10.1029/2009JD013638.

Gill, A. E., 1980: Some simple solutions for heat-induced tropical circulation. *Quart. J. Roy. Meteor. Soc.*, **106**, 447–462, https://doi.org/10.1002/qj.49710644905.

Goss, M., and S. B. Feldstein, 2017: Why do similar patterns of tropical convection yield extratropical circulation anomalies of opposite sign? *J. Atmos. Sci.*, **74**, 487–511, https://doi.org/10.1175/JAS-D-16-0067.1.

Grise, K. M., and D. W. J. Thompson, 2012: Equatorial planetary waves and their signature in atmospheric variability. *J. Atmos. Sci.*, **69**, 857–874, https://doi.org/10.1175/JAS-D-11-0123.1.

——, and ——, 2013: On the signatures of equatorial and extratropical wave forcing in tropical tropopause layer temperatures. *J. Atmos. Sci.*, **70**, 1084–1102, https://doi.org/10.1175/JAS-D-12-0163.1.

Hamilton, K., 1993: An examination of observed Southern Oscillation effects in the Northern Hemisphere stratosphere. *J. Atmos. Sci.*, **50**, 3468–3474, https://doi.org/10.1175/1520-0469(1993)050<3468:AEOOSO>2.0.CO;2.

Hegglin, M. I., and Coauthors, 2014: Vertical structure of stratospheric water vapour trends derived from merged satellite data. *Nat. Geosci.*, **7**, 768–776, https://doi.org/10.1038/ngeo2236.

Highwood, E. J., and B. J. Hoskins, 1998: The tropical tropopause. *Quart. J. Roy. Meteor. Soc.*, **124**, 1579–1604, https://doi.org/10.1002/qj.49712454911.

Hoerling, M. P., A. Kumar, and M. Zhong, 1997: El Niño, La Niña, and the nonlinearity of their teleconnections. *J. Climate*, **10**, 1769–1786, https://doi.org/10.1175/1520-0442(1997)010<1769:ENOLNA>2.0.CO;2.

Holland, M. M., D. A. Bailey, B. P. Briegleb, B. Light, and E. Hunke, 2012: Improved sea ice shortwave radiation physics in CCSM4: The impact of melt ponds and aerosols on Arctic sea ice. *J. Climate*, **25**, 1413–1430, https://doi.org/10.1175/JCLI-D-11-00078.1.

Holton, J. R., and A. Gettelman, 2001: Horizontal transport and the dehydration of the stratosphere. *Geophys. Res. Lett.*, **28**, 2799–2802, https://doi.org/10.1029/2001GL013148.

——, P. H. Haynes, M. E. McIntyre, A. R. Douglass, R. B. Rood, and L. Pfister, 1995: Stratosphere-troposphere exchange. *Rev. Geophys.*, **33**, 403–439, https://doi.org/10.1029/95RG02097.

Hu, D. Z., W. S. Tian, F. Xie, J. C. Shu, and S. Dhomse, 2014: Effects of meridional sea surface temperature changes on stratospheric temperature and circulation. *Adv. Atmos. Sci.*, **31**, 888–900, https://doi.org/10.1007/s00376-013-3152-6.

——, ——, Z. Y. Guan, Y. P. Guo, and S. Dhomse, 2016: Longitudinal asymmetric trends of tropical cold-point tropopause temperature and their link to strengthened Walker circulation. *J. Climate*, **29**, 7755–7771, https://doi.org/10.1175/JCLI-D-15-0851.1.

Hurrell, J. W., and Coauthors, 2013: The Community Earth System Model: A framework for collaborative research. *Bull. Amer. Meteor. Soc.*, **94**, 1339–1360, https://doi.org/10.1175/BAMS-D-12-00121.1.

Ineson, S., and A. A. Scaife, 2009: The role of the stratosphere in the European climate response to El Niño. *Nat. Geosci.*, **2**, 32–36, https://doi.org/10.1038/ngeo381.

Jiang, J. H., N. J. Livesey, H. Su, L. Neary, J. C. McConnell, and N. A. D. Richards, 2007: Connecting surface emissions, convective uplifting, and long-range transport of carbon monoxide in the upper troposphere: New observations from the Aura Microwave Limb Sounder. *Geophys. Res. Lett.*, **34**, L18812, https://doi.org/10.1029/2007GL030638.

——, H. Su, C. Zhai, L. Wu, K. Minschwaner, A. M. Molod, and A. M. Tompkins, 2015: An assessment of upper troposphere and lower stratosphere water vapor in MERRA, MERRA2, and ECMWF reanalyses using Aura MLS observations. *J. Geophys. Res. Atmos.*, **120**, 11 468–11 485, https://doi.org/10.1002/2015JD023752.

Kao, H. Y., and J. Y. Yu, 2009: Contrasting eastern-Pacific and central-Pacific types of ENSO. *J. Climate*, **22**, 615–632, https://doi.org/10.1175/2008JCLI2309.1.

Kawatani, Y., J. N. Lee, and K. Hamilton, 2014: Interannual variations of stratospheric water vapor in MLS observations and climate model simulations. *J. Atmos. Sci.*, **71**, 4072–4085, https://doi.org/10.1175/JAS-D-14-0164.1.

Kirk-Davidoff, D. B., E. J. Hintsa, J. G. Anderson, and D. W. Keith, 1999: The effect of climate change on ozone depletion through changes in stratospheric water vapour. *Nature*, **402**, 399–401, https://doi.org/10.1038/46521.

Konopka, P., F. Ploeger, M. C. Tao, and M. Riese, 2016: Zonally resolved impact of ENSO on the stratospheric circulation and water vapor entry values. *J. Geophys. Res. Atmos.*, **121**, 11 486–11 501, https://doi.org/10.1002/2015JD024698.

Marsh, D. R., and R. R. García, 2007: Attribution of decadal variability in lower-stratospheric tropical ozone. *Geophys. Res. Lett.*, **34**, L21807, https://doi.org/10.1029/2007GL030935.

——, M. J. Mills, D. E. Kinnison, J. F. Lamarque, N. Calvo, and L. M. Polvani, 2013: Climate change from 1850 to 2005 simulated in CESM1(WACCM). *J. Climate*, **26**, 7372–7391, https://doi.org/10.1175/JCLI-D-12-00558.1.

Matsuno, T., 1966: Quasi-geostrophic motions in the equatorial area. *J. Meteor. Soc. Japan*, **44**, 25–42.

Matthews, A. J., B. J. Hoskins, and M. Masutani, 2004: The global response to tropical heating in the Madden–Julian oscillation during the northern winter. *Quart. J. Roy. Meteor. Soc.*, **130**, 1991–2011, https://doi.org/10.1256/qj.02.123.

O'Sullivan, D., and T. J. Dunkerton, 1997: The influence of the quasi-biennial oscillation on global constituent distributions. *J. Geophys. Res.*, **102**, 21 731–21 743, https://doi.org/10.1029/97JD01689.

Randel, W. J., and E. J. Jensen, 2013: Physical processes in the tropical tropopause layer and their roles in a changing climate. *Nat. Geosci.*, **6**, 169–176, https://doi.org/10.1038/ngeo1733.

——, F. Wu, J. M. Russell, A. Roche, and J. W. Waters, 1998: Seasonal cycles and QBO variations in stratospheric CH_4 and H_2O observed in *UARS* HALOE data. *J. Atmos. Sci.*, **55**, 163–185, https://doi.org/10.1175/1520-0469(1998)055<0163:SCAQVI>2.0.CO;2.

——, ——, H. Vömel, G. E. Nedoluha, and P. Forster, 2006: Decreases in stratospheric water vapor after 2001: Links to changes in the tropical tropopause and the Brewer–Dobson circulation. *J. Geophys. Res.*, **111**, D12312, https://doi.org/10.1029/2005JD006744.

——, R. R. García, N. Calvo, and D. Marsh, 2009: ENSO influence on zonal mean temperature and ozone in the tropical lower stratosphere. *Geophys. Res. Lett.*, **36**, L15822, https://doi.org/10.1029/2009GL039343.

Raval, A., and V. Ramanathan, 1989: Observational determination of the greenhouse effect. *Nature*, **342**, 758–761, https://doi.org/10.1038/342758a0.

Ren, R. C., M. Cai, C. Xiang, and G. Wu, 2012: Observational evidence of the delayed response of stratospheric polar vortex variability to ENSO SST anomalies. *Climate Dyn.*, **38**, 1345–1358, https://doi.org/10.1007/s00382-011-1137-7.

——, J. Rao, G. Wu, and M. Cai, 2017: Tracking the delayed response of the northern winter stratosphere to ENSO using multi reanalyses and model simulations. *Climate Dyn.*, **48**, 2859–2879, https://doi.org/10.1007/s00382-016-3238-9.

Rodwell, M. J., and B. J. Hoskins, 1996: Monsoons and the dynamics of deserts. *Quart. J. Roy. Meteor. Soc.*, **122**, 1385–1404, https://doi.org/10.1002/qj.49712253408.

Rosenlof, K. H., 2003: How water enters the stratosphere. *Science*, **302**, 1691–1692, https://doi.org/10.1126/science.1092703.

——, and G. C. Reid, 2008: Trends in the temperature and water vapor content of the tropical lower stratosphere: Sea surface connection. *J. Geophys. Res.*, **113**, D06107, https://doi.org/10.1029/2007JD009109.

——, and Coauthors, 2001: Stratospheric water vapor increases over the past half-century. *Geophys. Res. Lett.*, **28**, 1195–1198, https://doi.org/10.1029/2000GL012502.

Scaife, A. A., N. Butchart, D. R. Jackson, and R. Swinbank, 2003: Can changes in ENSO activity help to explain increasing stratospheric water vapor? *Geophys. Res. Lett.*, **30**, 1880, https://doi.org/10.1029/2003GL017591.

Schieferdecker, T., S. Lossow, G. P. Stiller, and T. von Clarmann, 2015: Is there a solar signal in lower stratospheric water vapour? *Atmos. Chem. Phys.*, **15**, 9851–9863, https://doi.org/10.5194/acp-15-9851-2015.

Sherwood, S. C., and A. E. Dessler, 2000: On the control of stratospheric humidity. *Geophys. Res. Lett.*, **27**, 2513–2516, https://doi.org/10.1029/2000GL011438.

Shindell, D. T., 2001: Climate and ozone response to increased stratospheric water vapor. *Geophys. Res. Lett.*, **28**, 1551–1554, https://doi.org/10.1029/1999GL011197.

Simmons, A., S. Uppala, and D. Dee, 2007a: Update on ERA-Interim. *ECMWF Newsletter*, No. 111, ECMWF, Reading, United Kingdom, 5.

——, ——, ——, and S. Kobayashi, 2007b: ERA-Interim: New ECMWF reanalysis products from 1989 onwards. *ECMWF Newsletter*, No. 110, ECMWF, Reading, United Kingdom, 25–35, https://doi.org/10.21957/pocnex23c6.

Solomon, S., K. H. Rosenlof, R. W. Portmann, J. S. Daniel, S. M. Davis, T. J. Sanford, and G. K. Plattner, 2010: Contributions of stratospheric water vapor to decadal changes in the rate of global warming. *Science*, **327**, 1219–1223, https://doi.org/10.1126/science.1182488.

Son, S. W., and Coauthors, 2008: The impact of stratospheric ozone recovery on the Southern Hemisphere westerly jet. *Science*, **320**, 1486–1489, https://doi.org/10.1126/science.1155939.

——, and Coauthors, 2010: Impact of stratospheric ozone on Southern Hemisphere circulation change: A multimodel assessment. *J. Geophys. Res.*, **115**, D00M07, https://doi.org/10.1029/2010JD014271.

Stenke, A., and V. Grewe, 2005: Simulation of stratospheric water vapor trends: Impact on stratospheric ozone chemistry. *Atmos. Chem. Phys.*, **5**, 1257–1272, https://doi.org/10.5194/acp-5-1257-2005.

Su, H., W. G. Read, J. H. Jiang, J. W. Waters, D. L. Wu, and E. J. Fetzer, 2006: Enhanced positive water vapor feedback associated with tropical deep convection: New evidence from Aura MLS. *Geophys. Res. Lett.*, **33**, L05709, https://doi.org/10.1029/2005GL025505.

Tian, W. S., M. Chipperfield, and D. R. Lü, 2009: Impact of increasing stratospheric water vapor on ozone depletion and temperature change. *Adv. Atmos. Sci.*, **26**, 423–437, https://doi.org/10.1007/s00376-009-0423-3.

——, M. P. Chipperfield, D. S. Stevenson, R. Damoah, S. Dhomse, A. Dudhia, H. Pumphrey, and P. Bernath, 2010: Effects of stratosphere-troposphere chemistry coupling on tropospheric ozone. *J. Geophys. Res.*, **115**, D00M04, https://doi.org/10.1029/2009JD013515.

Tompkins, A. M., 2001: On the relationship between tropical convection and sea surface temperature. *J. Climate*, **14**, 633–637, https://doi.org/10.1175/1520-0442(2001)014<0633:OTRBTC>2.0.CO;2.

Uppala, S., D. Dee, S. Kobayashi, P. Berrisford, and A. Simmons, 2008: Towards a climate data assimilation system: Status update of ERA-Interim. *ECMWF Newsletter*, No. 115, ECMWF, Reading, United Kingdom, 12–18, https://doi.org/10.21957/byinox4wot.

Virts, K. S., and J. M. Wallace, 2010: Annual, interannual, and intraseasonal variability of tropical tropopause transition layer cirrus. *J. Atmos. Sci.*, **67**, 3097–3112, https://doi.org/10.1175/2010JAS3413.1.

Wang, T., W. J. Randel, A. E. Dessler, M. R. Schoeberl, and D. E. Kinnison, 2014: Trajectory model simulations of ozone (O_3) and carbon monoxide (CO) in the lower stratosphere. *Atmos. Chem. Phys.*, **14**, 7135–7147, https://doi.org/10.5194/acp-14-7135-2014.

——, A. Dessler, M. Schoeberl, W. Randel, and J.-E. Kim, 2015: The impact of temperature vertical structure on trajectory modeling of stratospheric water vapor. *Atmos. Chem. Phys.*, **15**, 3517–3526, https://doi.org/10.5194/acp-15-3517-2015.

Wang, W. K., K. Matthes, T. Schmidt, and L. Neef, 2013: Recent variability of the tropical tropopause inversion layer. *Geophys. Res. Lett.*, **40**, 6308–6313, https://doi.org/10.1002/2013GL058350.

——, ——, and ——, 2015: Quantifying contributions to the recent temperature variability in the tropical tropopause layer. *Atmos. Chem. Phys.*, **15**, 5815–5826, https://doi.org/10.5194/acp-15-5815-2015.

——, ——, N. E. Omrani, and M. Latif, 2016: Decadal variability of tropical tropopause temperature and its relationship to the Pacific decadal oscillation. *Sci. Rep.*, **6**, 29537, https://doi.org/10.1038/srep29537.

Watanabe, M., 2004: Asian jet waveguide and a downstream extension of the North Atlantic Oscillation. *J. Climate*, **17**, 4674–4691, https://doi.org/10.1175/JCLI-3228.1.

——, and M. Kimoto, 2000: Atmosphere-ocean thermal coupling in the North Atlantic: A positive feedback. *Quart. J. Roy. Meteor. Soc.*, **126**, 3343–3369, https://doi.org/10.1002/qj.49712657017.

WMO, 2003: Scientific assessment of ozone depletion: 2002. Global Ozone Research and Monitoring Project Rep. 47, 498 pp., https://www.wmo.int/pages/prog/arep/gaw/ozone_2002/ozone_2002.html.

Xie, F., W. Tian, J. Austin, J. Li, H. Tian, J. Shu, and C. Chen, 2011: The effect of ENSO activity on lower stratospheric water vapor. *Atmos. Chem. Phys. Discuss.*, **11**, 4141–4166, https://doi.org/10.5194/acpd-11-4141-2011.

——, J. Li, W. Tian, J. Feng, and Y. Huo, 2012: Signals of El Niño Modoki in the tropical tropopause layer and stratosphere. *Atmos. Chem. Phys.*, **12**, 5259–5273, https://doi.org/10.5194/acp-12-5259-2012.

——, and Coauthors, 2016: A connection from Arctic stratospheric ozone to El Nino–Southern Oscillation. *Environ. Res. Lett.*, **11**, 124026, https://doi.org/10.1088/1748-9326/11/12/124026.

Yan, X. H., C. R. Ho, Q. Zheng, and V. Klemas, 1992: Temperature and size variabilities of the western Pacific warm pool. *Science*, **258**, 1643–1645, https://doi.org/10.1126/science.258.5088.1643.

Yu, J. Y., and H. Y. Kao, 2007: Decadal changes of ENSO persistence barrier in SST and ocean heat content indices: 1958–2001. *J. Geophys. Res.*, **112**, D13106, https://doi.org/10.1029/2006JD007654.

Zhang, J., W. S. Tian, M. P. Chipperfield, F. Xie, and J. Huang, 2016: Persistent shift of the Arctic polar vortex towards the Eurasian continent in recent decades. *Nat. Climate Change*, **6**, 1094–1099, https://doi.org/10.1038/nclimate3136.

Zhou, X., J. Li, F. Xie, R. Ding, Y. Li, S. Zhao, J. Zhang, and Y. Li, 2017: The effects of the Indo-Pacific warm pool on the stratosphere. *Climate Dyn.*, https://doi.org/10.1007/s00382-017-3584-2, in press.